

## Master Thesis

# Morphology Optimization of a Tilt-Rotor MAV

Spring Term 2018



# **Declaration of Originality**

I hereby declare that the written work I have submitted entitled

**Morphology Optimization of a Tilt-Rotor MAV**

is original work which I alone have authored and which is written in my own words.<sup>1</sup>

**Author(s)**

Luca Rinsoz

**Student supervisor(s)**

Karen Bodie  
Zachary Taylor

**Supervising lecturer**

Roland Siegwart

With the signature I declare that I have been informed regarding normal academic citation rules and that I have read and understood the information on 'Citation etiquette' (<https://www.ethz.ch/content/dam/ethz/main/education/rechtliches-abschluesse/leistungskontrollen/plagiarism-citationetiquette.pdf>). The citation conventions usual to the discipline in question here have been respected.

The above written work may be tested electronically for plagiarism.

---

Place and date

---

Signature

---

<sup>1</sup>Co-authored work: The signatures of all authors are required. Each signature attests to the originality of the entire piece of written work in its final form.

# Contents

<b>Abstract</b>	<b>iii</b>
<b>Symbols</b>	<b>v</b>
<b>1 Introduction</b>	<b>1</b>
<b>2 Method</b>	<b>3</b>
2.1 Modelisation of MAVs . . . . .	4
2.2 Optimization problem . . . . .	6
2.3 Optimization tool . . . . .	8
2.4 Simulation Approach . . . . .	10
<b>3 Optimization Results</b>	<b>11</b>
3.1 Platonic Solids . . . . .	11
3.2 Even Designs . . . . .	12
3.2.1 Quad-copter . . . . .	12
3.2.2 Hexa-copter . . . . .	13
3.2.3 Octa-copter . . . . .	14
3.3 Odd Designs . . . . .	15
3.3.1 Tri-copter . . . . .	15
3.3.2 Penta-copter . . . . .	16
3.3.3 Hepta-copter . . . . .	17
3.4 Comparison of Different Designs . . . . .	18
3.5 Results when n is an Optimization Parameter . . . . .	18
<b>4 Simulation Results</b>	<b>21</b>
4.1 Hexa-copter . . . . .	21
4.2 Hepta-copter . . . . .	21
4.3 Octa-copter . . . . .	21
<b>5 Conclusion</b>	<b>23</b>
5.1 Summary/Achieved . . . . .	23
5.2 Improvements . . . . .	23
5.3 Further Developement . . . . .	23
<b>Bibliography</b>	<b>25</b>
<b>Acknowledgements</b>	<b>27</b>
<b>A UML: Activity Diagram</b>	<b>29</b>

# Abstract

To select the morphology of an omni-directional platform with changing propeller axes is not a straightforward problem. Various factors influence the desired morphology, such as flight efficiency, omni-directionality, and control authority. In the present work the development of a tool that solves the design optimization problem for a tilt-rotor MAV is presented. Different optimal morphology are then acquired. Finally, a verification of the proposed platforms is then completed in different simulations.



# Symbols

## Symbols

$\phi, \theta, \psi$	roll, pitch and yaw angle
$\beta_{PS}$	platonic solid angle
$\beta_{arm,i}$	angle between horizontal plan and MAV's i-th arm
$\theta_{arm,i}$	angle formed by the MAV's i-th arm in the horizontal plan
$\mathcal{F}_W$	inertial world frame
$\mathcal{F}_B$	inertial body frame
$\mathcal{F}_{P_i}$	i-th propeller frame
$p$	position of the MAV in $\mathcal{F}_W$
$\omega_B$	angular velocity of the MAV in $\mathcal{F}_B$
${}^W R_B$	rotation matrix from $\mathcal{F}_B$ to $\mathcal{F}_W$
${}^B R_{P_i}$	rotation matrix from $\mathcal{F}_{P_i}$ to $\mathcal{F}_B$
$R_X(\gamma)$	canonical rotation matrix about the $X$ axis of angle $\gamma$
$R_Y(\gamma)$	canonical rotation matrix about the $Y$ axis of angle $\gamma$
$R_Z(\gamma)$	canonical rotation matrix about the $Z$ axis of angle $\gamma$
$\alpha_i$	i-th propeller tilt angle
$w_i$	i-th propeller rotation speed
$\tau_{ext_i}$	i-th propeller counter rotation torque
$T_i$	i-th thrust
$m$	total mass of the MAV
$I_B$	body inertia of the MAV
$n$	MAV's number of propellers
$L$	MAV's arms length
$\kappa_f$	propeller thrust coefficient
$\kappa_m$	propeller drag coefficient
$g$	gravity constant
$c(\gamma)$	cosine of the angle $\gamma$
$s(\gamma)$	sine of the angle $\gamma$

## Acronyms and Abbreviations

ccw	counterclockwise
cw	clockwise
CoM	Center of Mass

ETH	Eidgenössische Technische Hochschule
GUI	Graphical User Interface
MAD	Mean Absolute Deviation
MAV	Micro Aerial Vehicle
ROS	Robotic Operating System
sqp	sequential quadratic programming
UAV	Unmanned Aerial Vehicle
URDF	Unified Robot Description Format

# Chapter 1

## Introduction

Rotary wing micro aerial vehicles (MAVs) have been well studied in academia and found a lot of applications in the world such as search operations [1], photography [2] or even toys [3]. They encountered such a broad success because of their agility and mechanical simplicity. Nevertheless, traditional multi-rotor vehicles are under-actuated, which means that they cannot control their torque and force independently [4]. They are thus unable to change their position without changing their orientation.

Recently the focus has been on designing MAVs able to perform more complex tasks such as camera motion for the film industry [5] or bridge inspection where huge resources (i.e. cranes and large man-power) are needed. The ultimate goal would be for a drone to be able to interact with its surrounding and apply forces to it, in order to perform maintenance where humans can not access, or to do construction work in harsh environments.

To perform these tasks, an MAV has to be able to hover in any orientation, and for a proper disturbance rejection while manipulating, the drone must have the potential to accelerate instantaneously in any direction. Hence, the MAV has to be able to decouple its orientation and position control. A drone that has a decoupled force and torque control is referred to as an omni-directional MAV.

The problem of overcoming the under-actuation and achieving omni-directionality is not straightforward. To address this problem, several MAV designs have been presented over the past years. For instance, in [5], Voliro (name of the vehicle) is based on a traditional hexa-copter (see Figure 1.1). The omni-directionality issue is addressed by adding motors to rotate the thrusters around their arm axis, thus allowing a control not only of the thrust produced by each propeller, but also of the orientation of this thrust. This tilting rotor system allows for decoupling the control of position and orientation. By using a control scheme based on an allocation technique, the system provides very good maneuverability.



Figure 1.1: Voliro [5].

In [4], the Omnicopter (name of the vehicle) is described. It is a drone with eight fixed rotors and the drone shape is the result of a mathematical optimization which maximizes the vehicle's agility with the constraint that its dynamical properties would be as independent as possible on the vehicle's orientation (see Figure 1.2).

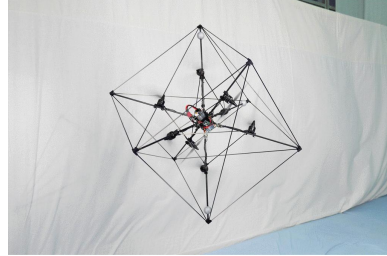


Figure 1.2: Omnicopter [4].

In [6], the MAV is a fixed propeller multi-rotor. The design is also the result of an optimization, which tends to minimize the body volume, to maximize the controllability of the system, avoid eventual aerodynamic interactions and to maximizes the efficiency in performing manipulation tasks.

The idea presented in [7] is a mix between Voliro and the Omnicopter because the design is a modified hexarotor, which achieves full control over the vehicle's position and orientation using manually tiltable propellers (see Figure 1.3). The paper also provides a methodology to optimize the fixed tilting angles depending on the desired trajectory.



Figure 1.3: Hexacopter with manually tilttable rotors [7].

Yet, nothing in the literature is found about the morphology optimization of MAVs with tilting rotors. Hence the need for the present research project. The aim of this thesis is thus to design a morphology optimization problem for a tilt-rotor MAV that accounts for the different factors that influence the morphology such as:

- Omni-directionality
- Flight efficiency
- Controlability

To reach this goal the chosen approach is to build an optimization tool that solves the optimization problem and returns different MAV designs. The most interesting designs are then tested in simulation. In this report the methods used to build the optimization tool and to simulate the results are discussed. Afterwards, the results returned by the tool are shown and compared based on different criteria. Finally, the results gathered during the simulation phase are also covered.

# Chapter 2

## Method

As explained in Chapter 1 the aim of this work is to find a drone design that is the result of an optimization problem, which tends to maximize the MAV's omnidirectionality, flight efficiency and controllability. In order to achieve this goal, it is, first of all, important to state which parameters will be used to define the design of an MAV. These parameters are defined as:

- $\beta_{arm}$  (angles formed by the arms with the horizontal plane see Figure 2.1)
- $\theta_{arm}$  (angles formed by the arms in the horizontal plane see Figure 2.1)
- $L$  (arm length)
- $n$  (number of propellers)

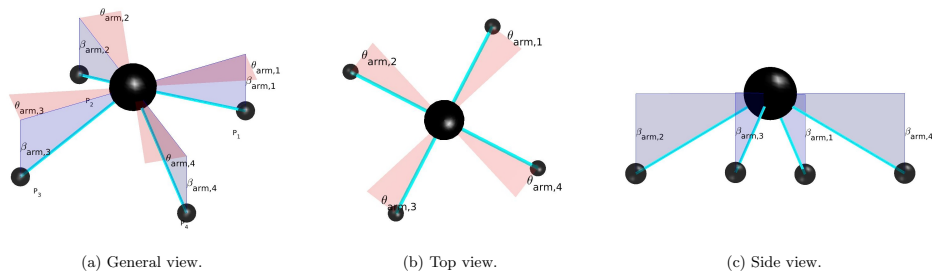


Figure 2.1: Arbitrary quad-copter design to illustrate the parameters that define the morphology of an MAV (with  $n = 4$ ,  $\beta_{arm} = [30^\circ, 30^\circ, 30^\circ, 30^\circ]$ ,  $\theta_{arm} = [22^\circ, 22^\circ, 22^\circ, 22^\circ]$ , and  $L = 0.4 [m]$ ).

To solve the problem, an optimization software or tool is developed with MATLAB<sup>®</sup><sup>1</sup>. This tool returns the aforementioned parameters along with other information on the corresponding MAV design. The interesting drone designs which result from the tool are then simulated on Gazebo<sup>®</sup><sup>2</sup> and the control of the different models is achieved using a Robotic Operating System<sup>3</sup> (ROS) node.

This chapter first covers the theory needed to obtain a generalized mathematical model for a n-rotor MAV with an arbitrary morphology. Then, the optimization problem is defined. Afterwards, the optimization tool is described. In the end, the theoretical background needed to perform the simulations is covered.

<sup>1</sup>A numerical computing environment and programming language developed by MathWorks<sup>®</sup> [8].

<sup>2</sup>An open source robot simulation software [9].

<sup>3</sup>An open source collection of software that help developers to create robot applications [10].

## 2.1 Modelisation of MAVs

In the following part, a dynamical model for a general design of an MAV is presented. Such a modelisation is needed to mathematically optimize the morphology of an MAV. This model is inspired by the models presented in [5] and [11].

### Assumptions

In this model, the first assumption is that the MAV is composed of  $n+1$  rigid bodies: one for each propeller unit  $P_i$  and one for the body  $B$ . Then, it is considered that the thrust is produced by irreversible fixed-pitch motor-propeller actuators. Finally, only the aerodynamic forces and torques that are responsible for the MAV actuation are considered, all the second order effects and disturbances are neglected as well as the airflow interactions between the rotors are neglected.

### Initial Definitions

In order to understand correctly the dynamical model, a few definitions are needed. First, let us define  $\mathcal{F}_W : \{O_W; X_W, Y_W, Z_W\}$  as the world fixed inertial frame and  $\mathcal{F}_B : \{O_B, X_B, Y_B, Z_B\}$  as a moving frame attached to the MAV. Also,  $\mathcal{F}_{P_i} : \{O_{P_i}; X_{P_i}, Y_{P_i}, Z_{P_i}\}, i = 1 \dots n$  is the frame of the  $i$ -th propeller. The propeller rotates around the axis  $Z_{P_i}$ , and thus the thrust  $T_i$  is produced along this axis. The tilt movement of the rotors is a simple rotation around  $X_{P_i}$ . Now let  ${}^W R_B$  be the orientation of the body frame with respect to the world frame and  ${}^B R_{P_i}$  be the orientation of the  $i$ -th propeller with respect to the body frame. It is straightforward with the help of Figure 2.2 that

$${}^B R_{P_i} = R_Z \left( (i-1) \frac{2\pi}{n} \right) R_Z(\theta_{arm,i}) R_Y(\beta_{arm,i}) R_X(\alpha_i), \quad i = 1 \dots n. \quad (2.1)$$

Equivalently, let

$${}^B O_{P_i} = R_Z \left( (i-1) \frac{2\pi}{n} \right) R_Z(\theta_{arm,i}) R_Y(\beta_{arm,i}) \begin{bmatrix} L \\ 0 \\ 0 \end{bmatrix}, \quad i = 1 \dots n \quad (2.2)$$

be the origin of the  $i$ -th propeller frame  $\mathcal{F}_{P_i}$ . In Equation (2.1) and (2.2),  $(i-1) \frac{2\pi}{n}$  is the angle that the  $i$ -th arm would form with axis  $X_B$  if the arms of the drone are evenly distributed in the horizontal plane,  $\theta_{arm,i}$  is the angle that  $i$ -th arm forms in the horizontal plane with respect to its evenly distributed position (see Figure 2.1),  $\beta_{arm,i}$  is the angle that the  $i$ -th arm forms with the horizontal plane (see Figure 2.1),  $\alpha_i$  is the tilting angle of the  $i$ -th propeller about the  $X_{P_i}$  axis,  $L$  is the arm length and  $n$  is the number of propellers.

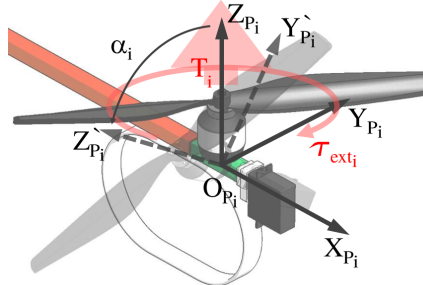


Figure 2.2: Representation of the  $i$ -th tilting arm [11].

### Equations of motion

Using Newton-Euler formalism, the general equations of motion of the MAV are

$$\begin{cases} \dot{\omega}_B = I_B^{-1} \sum_{i=1}^n ({}^B R_{P_i} \tau_{ext,i} + \tau_{Bi}) , \\ \ddot{p} = \begin{bmatrix} 0 \\ 0 \\ -g \end{bmatrix} \frac{1}{m} {}^W R_B \sum_{i=1}^n T_i . \end{cases} \quad (2.3)$$

Where

$$\tau_{Bi} = {}^B O_{P_i} \times {}^B R_{P_i} T_{P,i} , \quad (2.4)$$

$$\tau_{ext,i} = [0, 0, -c_i \kappa_m w_i^2]^T , \quad (2.5)$$

$$\begin{cases} c_i = 1, & \text{if } i \text{ is odd (cw rotation to produce + thrust)} \\ c_i = -1 & \text{if } i \text{ is even (ccw rotation to produce + thrust)} \end{cases}$$

and

$$T_i = {}^B R_{P_i} T_{P,i} , \quad T_{P,i} = [0, 0, \kappa_f w_i^2]^T . \quad (2.6)$$

In Equation (2.3)  $g$  is the gravity constant, in Equation (2.5)  $\kappa_m$  is the propeller drag coefficient, in Equation (2.6)  $\kappa_f$  is the propeller thrust coefficient and in Equations (2.5) and (2.6)  $w_i$  is the  $i$ -th propeller rotation speed. The force and torque that the drone produces in body frame  $\mathcal{F}_B$  are

$$\begin{bmatrix} M_B \\ F_B \end{bmatrix} = \left[ \sum_{i=1}^n ({}^B R_{P_i} \tau_{ext,i} + \tau_{Bi}) \right] , \quad (2.7)$$

that can be rewritten

$$\begin{bmatrix} M_B \\ F_B \end{bmatrix} = A(\alpha) W . \quad (2.8)$$

Where  $W = [w_1^2, w_2^2, \dots, w_n^2]$  and

$$A(\alpha) = \begin{bmatrix} (-\kappa_f L s(\beta_{arm,1}) c(\theta_{arm,1}) + c_1 \kappa_m s(\theta_{arm,1})) s(\alpha_1) + (\kappa_f L s(\theta_{arm,1}) + c_1 \kappa_m c(\theta_{arm,1}) s(\beta_{arm,1})) c(\alpha_1) & \dots \\ (-\kappa_f L s(\beta_{arm,1}) s(\theta_{arm,1}) - c_1 \kappa_m c(\theta_{arm,1}) s(\alpha_1) + (-\kappa_f L c(\theta_{arm,1}) + c_1 \kappa_m s(\beta_{arm,1}) s(\theta_{arm,1})) c(\alpha_1)) & \dots \\ (-L \kappa_f c(\beta_{arm,1})) s(\alpha_1) + (c_1 \kappa_m c(\beta_{arm,1})) c(\alpha_1) & \dots \\ s(\theta_{arm,1}) \kappa_f s(\alpha_1) + s(\beta_{arm,1}) c(\theta_{arm,1}) \kappa_f c(\alpha_1) & \dots \\ -c(\theta_{arm,1}) \kappa_f s(\alpha_1) + s(\beta_{arm,1}) s(\theta_{arm,1}) \kappa_f c(\alpha_1) & \dots \\ c(\beta_{arm,1}) \kappa_f c(\alpha_1) & \dots \end{bmatrix}$$

is the  $6 \times n$  allocation matrix and  $c(\cdot)$  and  $s(\cdot)$  represent the cosine and sine operator respectively.

### Static allocation

The optimization tool has to compute the maximal reachable force and torque in a large number of directions. So to compute that in a reasonable time in [5] an approach to transform the non-linear allocation matrix into a static allocation matrix, which renders the problem of inverse kinematic linear, is presented. To do so, the system in Equation (2.8) is rewritten as

$$\begin{bmatrix} M_B \\ F_B \end{bmatrix} = A_{static} F_{dec} . \quad (2.9)$$

Where  $F_{dec}$  is the decomposed force vector defined as follow

$$F_{dec} = \begin{pmatrix} F_{h,1} \\ F_{v,1} \\ \dots \\ F_{h,n} \\ F_{v,n} \end{pmatrix}, \quad (2.10)$$

with  $F_{v,1} = \kappa_f \cos(\alpha_i)$  the vertical force produced by the i-th propeller and  $F_{h,1} = \kappa_f \sin(\alpha_i)$  the horizontal force produced by the i-th propeller. And the static matrix defined as

$$A_{static} = \begin{bmatrix} -\kappa_f L s(\beta_{arm,1}) c(\theta_{arm,1}) + c_1 \kappa_m s(\theta_{arm,1}) & +\kappa_f L s(\theta_{arm,1}) + c_1 \kappa_m c(\theta_{arm,1}) s(\beta_{arm,1}) & \dots & \dots \\ -\kappa_f L s(\beta_{arm,1}) s(\theta_{arm,1}) - c_1 \kappa_m c(\theta_{arm,1}) & -\kappa_f L c(\theta_{arm,1}) + c_1 \kappa_m s(\beta_{arm,1}) s(\theta_{arm,1}) & \dots & \dots \\ -L \kappa_f c(\beta_{arm,1}) & c_1 \kappa_m c(\beta_{arm,1}) & \dots & \dots \\ s(\theta_{arm,1}) \kappa_f & s(\beta_{arm,1}) c(\theta_{arm,1}) \kappa_f & \dots & \dots \\ -c(\theta_{arm,1}) \kappa_f & s(\beta_{arm,1}) s(\theta_{arm,1}) \kappa_f & \dots & \dots \\ 0 & c(\beta_{arm,1}) \kappa_f & \dots & \dots \end{bmatrix}$$

a  $6 \times 2n$  matrix that is invariant for a drone design. Using the Moore-Penrose pseudo inverse we can easily get the inverse kinematic as

$$F_{dec} = A_{static}^\dagger \begin{bmatrix} M_{des} \\ F_{des} \end{bmatrix}. \quad (2.11)$$

Which returns the decomposed force vector for a desired force and torque. Finding the tilting angles and propellers rotation speed required to attain this desired force and torque is then

$$\begin{cases} w_i^2 = \frac{1}{\kappa_f} \sqrt{F_{v,i}^2 + F_{h,i}^2} \\ \alpha_i = \text{atan2}(F_{h,i}, F_{v,i}) \end{cases}. \quad (2.12)$$

## 2.2 Optimization problem

The following section focuses on the optimization problem that the tool has to solve in order to obtain a MAV design that is optimal. The criteria that make this design optimal are also discussed.

### Problem statement

The optimization problem is stated as follow

$$\arg \max_x f(x) \quad \text{subject to} \quad \begin{cases} c(x) \leq 0 \\ ceq(x) = 0 \\ A \cdot x \leq 0 \\ Aeq \cdot x = 0 \\ lb \leq x \leq ub, \end{cases} \quad (2.13)$$

where  $f(x)$  is the cost function,  $x$  the argument vector,  $c(x)$  the non-linear inequality constraint vector,  $ceq(x)$  the non-linear equality constraint vector,  $A$  the linear inequality constraint matrix,  $Aeq$  the linear equality constraint matrix,  $lb$  the lower bound vector of the arguments ( $x$ ) and  $ub$  the upper bound vector.

Once the optimization problem solved, the output is the optimal argument vector  $x^*$  that maximizes the cost function  $f(x)$ . In our case the argument vector  $x$  is composed of the MAV's morphology parameters ( $\beta_{arm}$ ,  $\theta_{arm}$ ,  $L$ ,  $n$ ) and the cost functions are the subject of the next section.

### Cost Functions

As stated in Chapter 1, the aim of the project is to obtain a multi-rotor design that is omni-directional. Therefore, it is the heart of the problem to define meaningful cost functions for the optimization problem, which when solved will return parameters for an omni-directional drone. In this section, the few cost functions that capture the omni-directionality are described.

The first cost function consists in maximizing the minimal attainable force and the minimal attainable torque that the MAV can produce in any direction. The omni-directionality is defined as the drone capacity to accelerate instantaneously in every direction. In order to do that the MAV has to have high minimal attainable force and torque, hence this cost function. It turns out that this cost function is also computationally less demanding for the solver than the others. Indeed, when the multi-rotors applies a force or torque in the direction parallel to one of its arms, the propeller on this arm is perfectly unable to produce any force or torque in this direction. This is due to the fact that no matter what the tilting angle for this propeller is, the thrust it produces is parallel to the arm direction (see Figure 2.2). Therefore, the minimal attainable forces and torques for the drone are in the direction towards which one of the propeller can't apply any thrust, i.e. the arm directions. So instead of optimizing the force and torque in a large number of direction, it is enough for this cost function to optimize the force and torque in  $n$  directions.

The second cost function consist of maximizing the minimal attainable force and the minimal attainable torque that the MAV can produce in any direction and minimizing the MAV's inertia. It is the same as the first cost function, but the last term is added in order to have an easier drone to control and thus add a criterion on the controllability.

The next cost function is designed to maximize the volume of the reachable force and torque space. The force and torque spaces are two polyhedrons formed by the drone's attainable forces and torques in every direction (see Figure 2.4a and Figure 2.4b). The idea behind this cost function is to have the biggest task space for the drone and hence increase the MAV's ability to navigate in any orientation and to any position. This cost function is computationally heavy for the solver, because in order to have precise polyhedrons for the different spaces, the forces and torques have to be computed in at least 578 directions.

Another cost function that maximizes the force, the torque and the hover efficiency in all directions is developed. The aim of this cost function is to maximize the agility of the MAV for good disturbance rejection. Moreover, the term that maximizes the hover efficiency is designed to give the drone the ability to perform manipulation efficiently in any orientation. Solving the optimization problem for this cost function can also be computationally heavy depending on how many effective directions you choose to represent “all directions”.

The last cost function maximizes the force and the torque in one defined direction  $d$ . It is mostly designed to test the optimization tool as it is computationally light and, given specific directions, the optimal design is pretty straightforward. For instance, if you maximize the force in the  $Z$  direction for a 4-rotors MAV, the expected optimal solution would be a traditional quad-copter. The presented cost functions use the multi-rotor model described in Section 2.1 to compute the different forces and torques in the different directions.

### Solver

To solve the problem in Equation (2.13), the tool uses the MATLAB<sup>®</sup> function fmincon, with different algorithms. The one showing the quickest convergence and

the best results being the sequential quadratic programming (sqp) algorithm.

## 2.3 Optimization tool

As explained above, an optimization tool has been developed to perform the design optimization of the drone and return information on the resulting design. In this section the tool is exposed and its working principle is explained.

### User Guide

To use the tool, the graphical user interface (GUI) represented in Figure 2.3 first has to be opened. Then, the parameters to optimize have to be selected. The choice is between optimizing just  $\beta_{arm}$  angles, or  $\beta_{arm}$  angles with other selected parameters (see Figure 2.3). Afterwards, the design parameters that are not selected for the optimization have to be specified. For instance, if the arm length is not to be optimized, the user has to specify an arm length. To solve the optimization the sqp algorithm needs an initial solution. Hence, an initial solution is expected from the user. Then the cost function has to be chosen from the list (see Figure 2.3). Finally, in order to obtain a result the user only needs to push the “start optimization” button.

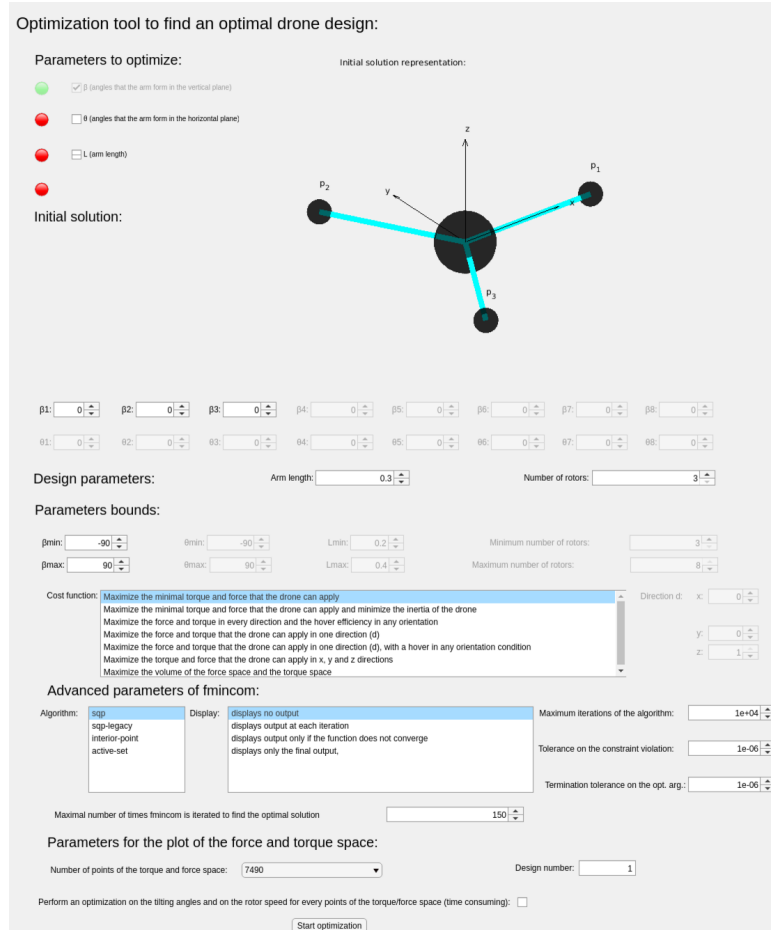


Figure 2.3: MAV morphology optimization tool GUI.

## Outcome

Apart from the optimal design parameters ( $\beta_{arm}$ ,  $\theta_{arm}$ ,  $L$  and  $n$ ), the optimization tool returns a MATLAB® plot containing the attainable force space, the attainable torque space, the hover efficiency in every orientation and a schematic of the MAV's design (see Figure 2.4). It is important to note that the force and torque space and the hover efficiency diagram are all represented in the drone's body frame. And thus, in the force and torque space diagrams, the dots that can be observed in Figure 2.4a represent directions equally distributed around the MAV's body center. The distance at which a point is with respect to the center of the body represents the magnitude of the maximal force or torque that the drone can apply in this direction. The color of this point represent the efficiency of the force or torque in this direction, calculated as

$$F_{eff} = \frac{\|Force_{attainable \text{ in } direction}\|}{\|Thrust_{produced \text{ in total}}\|}, M_{eff} = \frac{\|Torque_{attainable \text{ in } direction}\|}{\|L \cdot Thrust_{produced \text{ in total}}\|}.$$

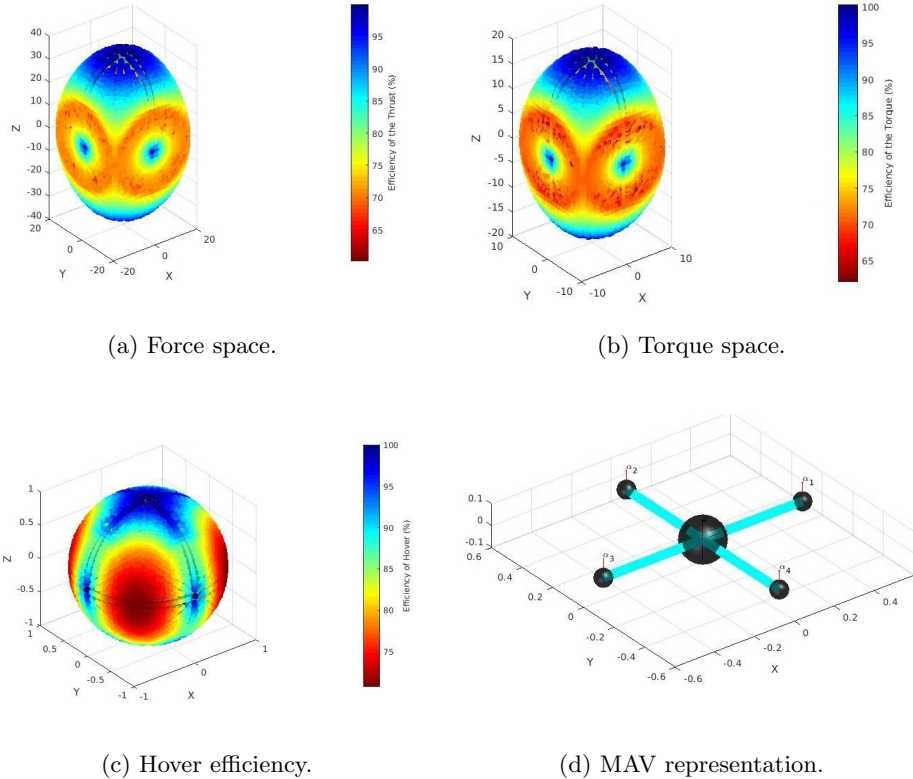


Figure 2.4: Example of the optimization tool's output.

Along with the design parameters and the figure the optimization tool also returns information on the drone capabilities called metrics. These metrics are listed in Table 2.1.

Table 2.1: List of the metrics returned by the optimization tool.

Metrics:	Minimal	Maximal	Mean	MAD	Task space volume	Task space surface
Force:	[N]	[N]	[N]	[N]	[ $N^3$ ]	[ $N^2$ ]
Torque:	[Nm]	[Nm]	[Nm]	[Nm]	[ $N^3 m^3$ ]	[ $N^2 m^2$ ]
Hover efficiency:	[%]	[%]	[%]	[%]	-	-

### Limitations

Due to the non-linearity of the cost functions and the fact that the algorithms available in MATLAB® only guarantee convergence to local optima, the solution returned by the tool is strongly dependent on the chosen initial solution. And also the more parameters one wants to be optimized the more the algorithms get stuck in local optima.

## 2.4 Simulation Approach

As said above, a few of the optimal designs are tested in simulation on Gazebo®. In order to be simulated on Gazebo® a robot model, which is represented in a Unified Robot Description Format<sup>4</sup> (URDF) file, is first launched on Gazebo®. In the mean time, a ROS node to control the robot's joints is also launched and the simulation can then properly start (see Figure 2.5). So as to simulate the chosen optimal MAV designs, they first have to be modeled in URDF files. Once that is done, the ROS node responsible for the control of the MAV, that is referred to as the control node, has to be built. The access to Voliro's control node was luckily granted during the present work [5]. Therefore, to properly control the different design of MAV obtained, only a few changes are needed on Voliro's control node. First, the controller node has to be generalized for a n-rotor drone (opposed to a 6-rotor drone for Voliro). Then, the static allocation matrix (which is how Voliro transforms a desired angular and linear acceleration into desired motor speeds and rotor tilting angles) has to be generalized to a n-rotor MAV with an arbitrary arm orientation. Finally, the arbitrary arm orientation can cause a center of mass (CoM) offset. An additional angular acceleration thus has to be added to the desired angular acceleration, in order to compensate for the CoM offset. This angular acceleration is calculated as follow

$$\dot{\omega}_{CoM} = -I_B^{-1}(R_{CoM} \times m\ddot{p}_{des}), \quad (2.14)$$

where  $R_{CoM}$  is the CoM position vector and  $\ddot{p}_{des}$  the desired linear acceleration. Once all these changes done, the MAV model can be controlled in Gazebo® as it can be seen in Figure 2.5).

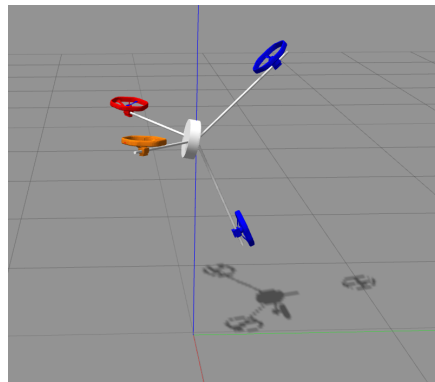


Figure 2.5: 4-rotors MAV design successfully launched and controlled in Gazebo®.

---

<sup>4</sup>Format based on XML used to represent robot models in ROS

# Chapter 3

# Optimization Results

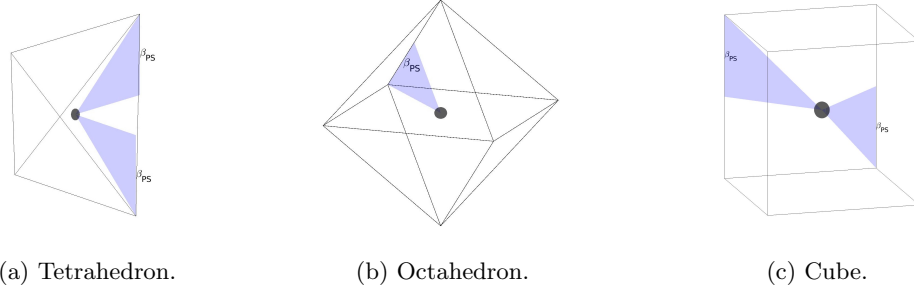
This chapter focuses on showing and analyzing the most interesting MAV designs outputted by the optimization tool. A short digression on platonic solid is first needed to properly analyse the results. The optimal designs with an even number of propellers are then described. Afterwards, the designs with an odd number of propellers are shown. A comparison of the different optimal drone design is then proposed. Finally, a few results of optimizations performed with the number of propeller as an argument are presented.

## 3.1 Platonic Solids

Platonic solids are five regular and convex polyhedrons named after the ancient Greek philosopher Plato to honor his memory [12]. The five platonic solids are:

- The tetrahedron composed of four faces and four vertices (see Figure 3.1a).
- The octahedron composed of eight faces and six vertices (see Figure 3.1b).
- The cube composed of six faces and eight vertices (see Figure 3.1c).
- The icosahedron composed of twenty faces and twelve vertices.
- The dodecahedron composed of twelve faces and twenty vertices.

There is a angle that can be found at least in the first three platonic solids. This angle is found between the horizontal plane and the vertices of the polyhedron (see Figure 3.1). To ensure simplicity, in the rest of this work this angle will be referred to as the platonic solids angle and  $\beta_{PS}$ .



(a) Tetrahedron. (b) Octahedron. (c) Cube.

Figure 3.1: The first three platonic solids ( $\cos(\beta_{PS}) = \sqrt{\frac{2}{3}} \Rightarrow \beta_{PS} \simeq 35.26^\circ$ ).

## 3.2 Even Designs

### 3.2.1 Quad-copter

Design 1:

- $n = 4$
- $\beta_{arm} = [35.26^\circ, -35.26^\circ, 35.26^\circ, -35.26^\circ]$
- $\theta_{arm} = [0^\circ, 0^\circ, 0^\circ, 0^\circ]$
- $L = 0.5 [m]$

Design 2:

- $n = 4$
- $\beta_{arm} = [-32.42^\circ, -35.49^\circ, -35.44^\circ, -35.49^\circ]$
- $\theta_{arm} = [-0.99^\circ, -1.88^\circ, -2.26^\circ, -2.94^\circ]$
- $L = 0.5 [m]$

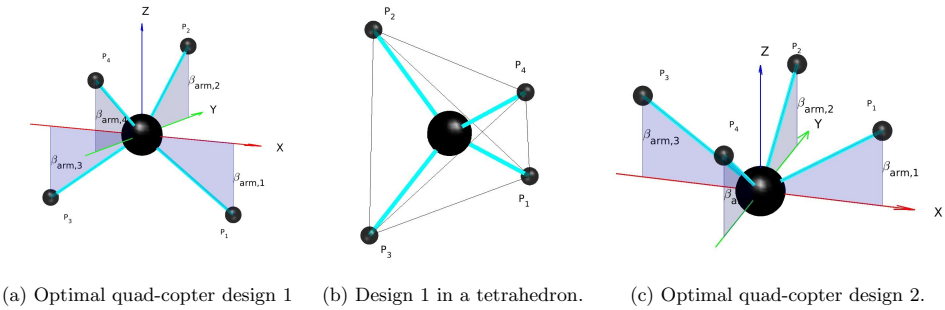


Figure 3.2: Schematic of the optimal designs obtained for the Quad-copter.

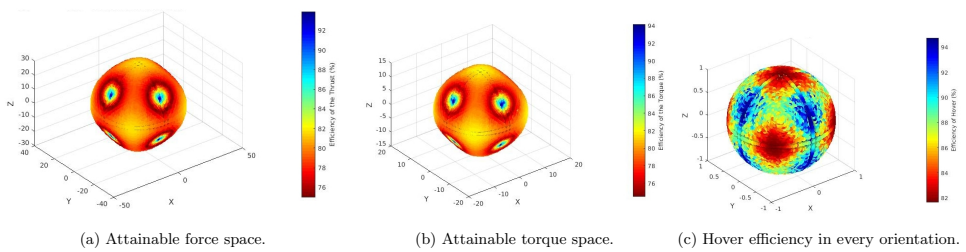


Figure 3.3: Representation of the capacities of Design 1.

Table 3.1: Comparison between the two designs' force capabilities.

Design	$F_{min} [N]$	$F_{max} [N]$	$F_{mean} [N]$	$MAD(F) [N]$	Force space volume [ $N^3$ ]	Force space surface [ $N^2$ ]
Design 1	23.23	28.37	26.87	0.86	81'710	9'326
Design 2	23.19	28.56	26.87	0.86	81'683	9'345

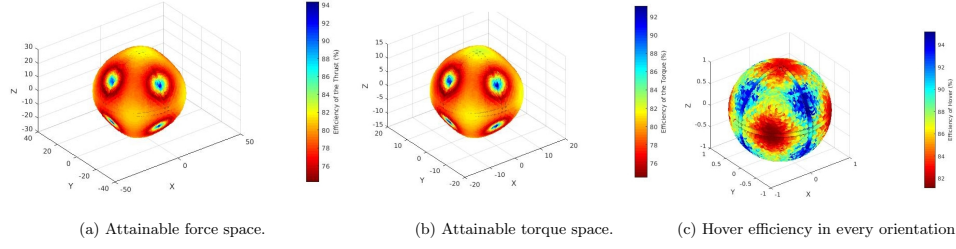


Figure 3.4: Representation of the capacities of Design 2.

Table 3.2: Comparison between the two designs' torque capabilities.

Design	$M_{min}$ [Nm]	$M_{max}$ [Nm]	$M_{mean}$ [Nm]	$MAD(M)$ [Nm]	Torque space volume [ $N^3 m^3$ ]	Torque space surface [ $N^2 m^2$ ]
Design 1	11.65	14.23	13.47	0.43	10'300	2'348
Design 2	11.62	14.32	13.47	0.43	10'298	2'355

Table 3.3: Comparison between the two designs' hover capabilities.

Design	$H_{eff,min}$ [%]	$H_{eff,max}$ [%]	$H_{eff,mean}$ [%]	$MAD(H_{eff})$ [%]
Design 1	81.65	94.73	87.1	2.6
Design 2	81.11	95.18	87.03	2.63

### 3.2.2 Hexa-copter

Optimal hexa-copter:

- $n = 6$
- $\beta_{arm} = [35.26^\circ, -35.26^\circ, 35.26^\circ, -35.26^\circ, 35.26^\circ, -35.26^\circ]$
- $\theta_{arm} = [0^\circ, 0^\circ, 0^\circ, 0^\circ, 0^\circ, 0^\circ]$
- $L = 0.5$  [m]

Voliro:

- $n = 6$
- $\beta_{arm} = [0^\circ, 0^\circ, 0^\circ, 0^\circ, 0^\circ, 0^\circ]$
- $\theta_{arm} = [0^\circ, 0^\circ, 0^\circ, 0^\circ, 0^\circ, 0^\circ]$
- $L = 0.5$  [m]

Table 3.4: Comparison between the two designs' force capabilities.

Design	$F_{min}$ [N]	$F_{max}$ [N]	$F_{mean}$ [N]	$MAD(F)$ [N]	Force space volume [ $N^3$ ]	Force space surface [ $N^2$ ]
Optimal hexa-copter	34.74	42.55	39.52	2.21	267'010	20'922
Voliro	26.6	52.11	37.77	4.33	244'293	20'170

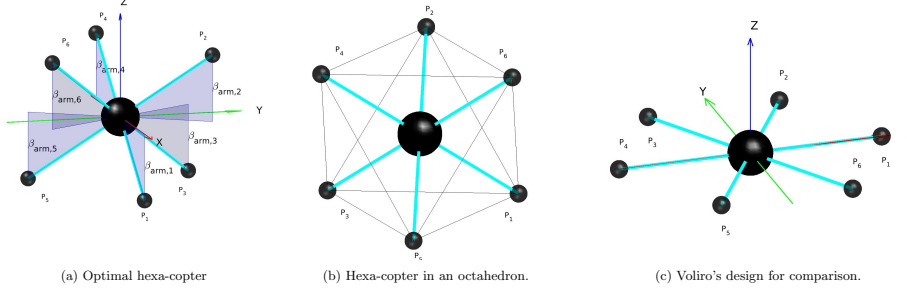


Figure 3.5: Schematic of the different possible designs for an Hexa-copter.

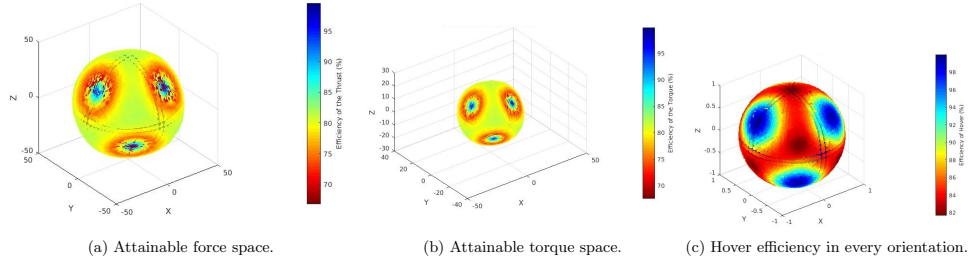


Figure 3.6: Representation of the capacities of the optimal hexa-copter.

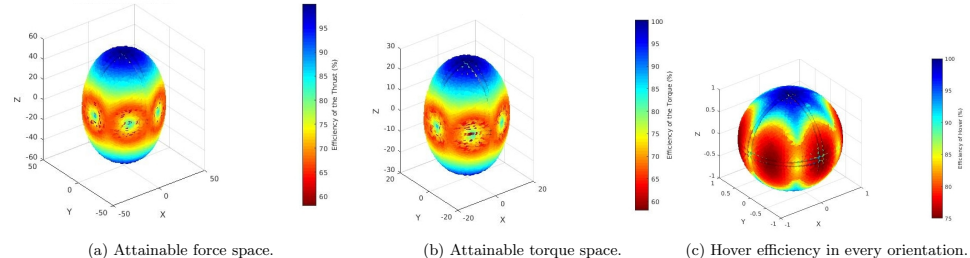


Figure 3.7: Representation of the capacities of Voliro.

Table 3.5: Comparison between the two designs' torque capabilities.

Design	$M_{min}$ [Nm]	$M_{max}$ [Nm]	$M_{mean}$ [Nm]	$MAD(M)$ [Nm]	Torque space volume [ $N^3 m^3$ ]	Torque space surface [ $N^2 m^2$ ]
Optimal hexa-copter	17.42	21.34	19.82	1.1	33'687	5'230
Voliro	15.09	26.13	18.94	2.17	30'788	5'121

Table 3.6: Comparison between two designs' hover capabilities.

Design	$H_{eff,min}$ [%]	$H_{eff,max}$ [%]	$H_{eff,mean}$ [%]	$MAD(H_{eff})$ [%]
Optimal hexa-copter	81.65	100	88.92	4.43
Voliro	75	100	84.21	5.35

### 3.2.3 Octa-copter

Optimal octa-copter:

- $n = 8$
- $\beta_{arm} = [35.26^\circ, -35.26^\circ, 35.26^\circ, -35.26^\circ, 35.26^\circ, -35.26^\circ, 35.26^\circ, -35.26^\circ]$

- $\theta_{arm} = [0^\circ, 0^\circ, 0^\circ, 0^\circ, 0^\circ, 0^\circ, 0^\circ, 0^\circ]$
- $L = 0.5 [m]$

Omnicopter:

- $n = 8$
- $\beta_{arm} = [-35.26^\circ, -35.26^\circ, -35.26^\circ, -35.26^\circ, 35.26^\circ, 35.26^\circ, 35.26^\circ, 35.26^\circ]$
- $\theta_{arm} = [0^\circ, 45^\circ, 90^\circ, 135^\circ, 180^\circ, -135^\circ, -90^\circ, -45^\circ]$
- $L = 0.5 [m]$

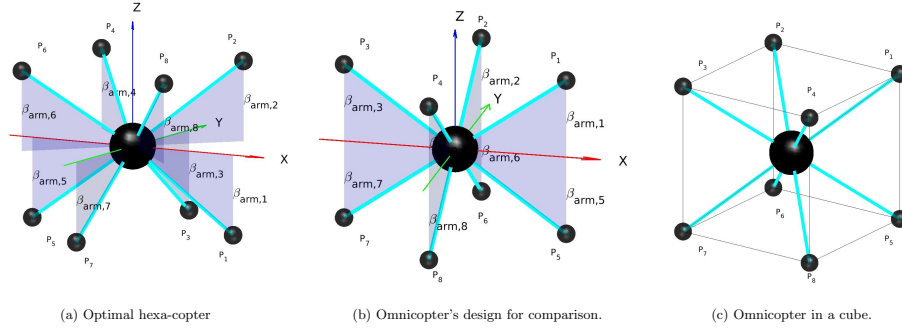


Figure 3.8: Schematic of the differnt possible designs for an Octa-copter.

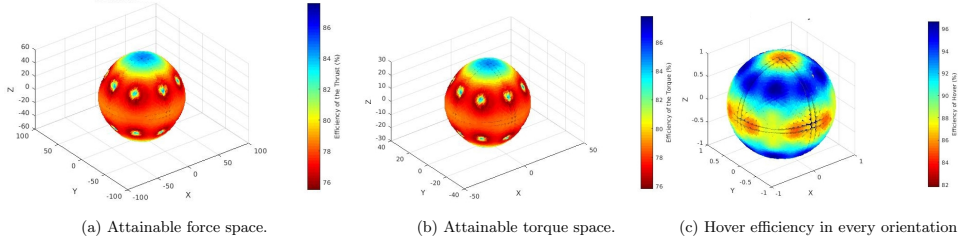


Figure 3.9: Representation of the capacities of the optimal octa-copter.

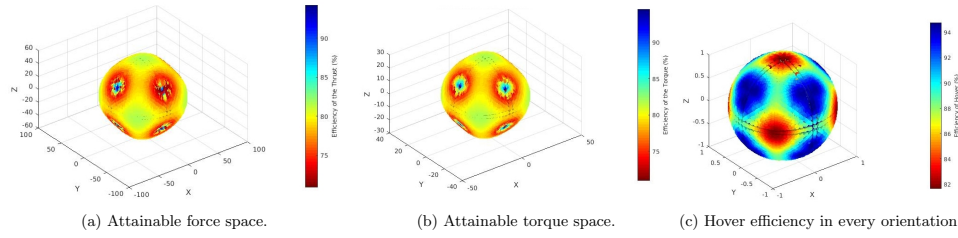


Figure 3.10: Representation of the capacities of Omnicopter.

### 3.3 Odd Designs

#### 3.3.1 Tri-copter

Optimal tri-copter:

Table 3.7: Comparison between the two designs' force capabilities.

Design	$F_{min}$ [N]	$F_{max}$ [N]	$F_{mean}$ [N]	$MAD(F)$ [N]	Force space volume [ $N^3$ ]	Force space surface [ $N^2$ ]
Optimal octa-copter	44.7	58.78	53.95	0.94	669'339	37'625
Omnicopter	46.46	56.73	53.75	1.72	653'736	37'263

Table 3.8: Comparison between the two designs' torque capabilities.

Design	$M_{min}$ [Nm]	$M_{max}$ [Nm]	$M_{mean}$ [Nm]	$MAD(M)$ [Nm]	Torque space volume [ $N^3 \cdot m^3$ ]	Torque space surface [ $N^2 \cdot m^2$ ]
Optimal octa-copter	22.4	29.48	27	0.47	84'417	9'463
Omnicopter	23.3	28.45	26.95	0.86	82'446	9'374

Table 3.9: Comparison between two designs' hover capabilities.

Design	$H_{eff,min}$ [%]	$H_{eff,max}$ [%]	$H_{eff,mean}$ [%]	$MAD(H_{eff})$ [%]
Optimal octa-copter	81.78	96.65	91.42	2.7
Omnicopter	81.64	94.77	89.36	2.82

- $n = 3$
- $\beta_{arm} = [35.26^\circ, 35.26^\circ, 35.26^\circ]$
- $\theta_{arm} = [0^\circ, 0^\circ, 0^\circ]$
- $L = 0.5 [m]$

### 3.3.2 Penta-copter

Optimal penta-copter:

- $n = 5$
- $\beta_{arm} = [35.26^\circ, 35.26^\circ, 35.26^\circ, 35.26^\circ, 35.26^\circ]$
- $\theta_{arm} = [0^\circ, 0^\circ, 0^\circ, 0^\circ, 0^\circ]$
- $L = 0.5 [m]$

Standard penta-copter:

- $n = 5$
- $\beta_{arm} = [0^\circ, 0^\circ, 0^\circ, 0^\circ, 0^\circ]$
- $\theta_{arm} = [0^\circ, 0^\circ, 0^\circ, 0^\circ, 0^\circ]$
- $L = 0.5 [m]$

Table 3.10: Comparison between the two designs' force capabilities.

Design	$F_{min}$ [N]	$F_{max}$ [N]	$F_{mean}$ [N]	$MAD(F)$ [N]	Force space volume [ $N^3$ ]	Force space surface [ $N^2$ ]
Optimal	26.03	36.22	33.69	1.39	160'333	14'626
Standard	26.24	43.42	31.93	3.25	146'006	14'137

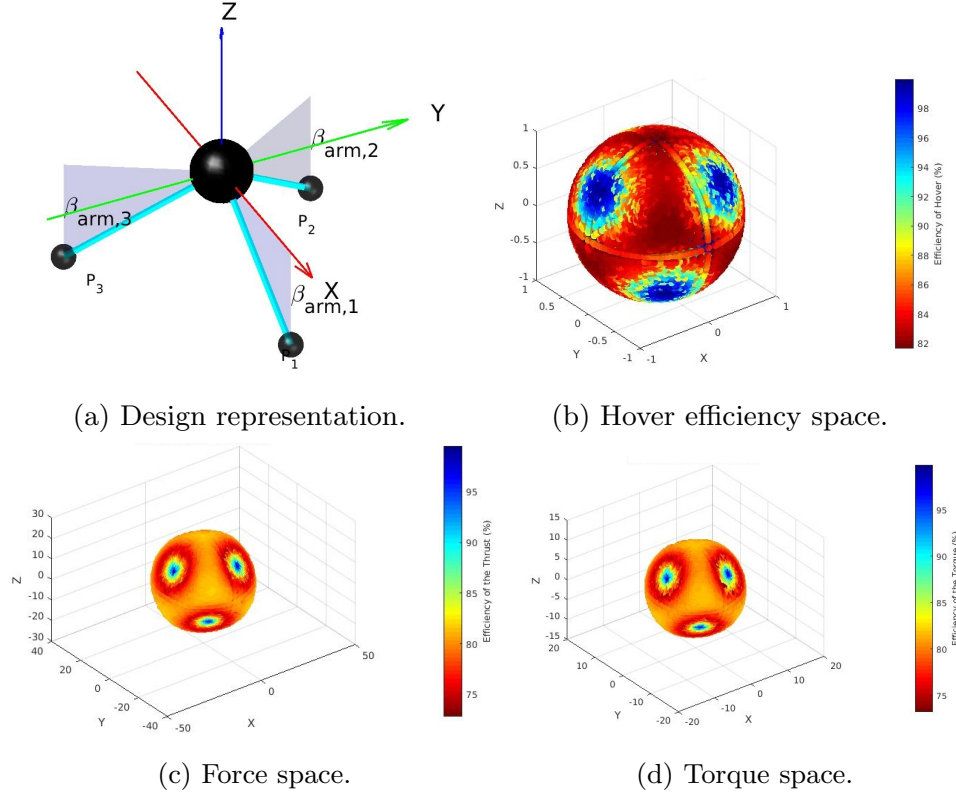


Figure 3.11: Visual representation of the optimal tri-copter capabilities.

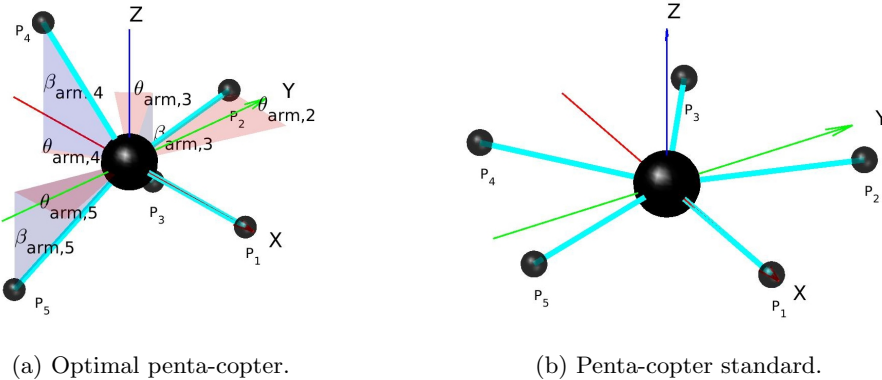


Figure 3.12: Schematic of different possible designs for a Penta-copter.

Table 3.11: Comparison between the two designs' torque capabilities.

Design	$M_{min}$ [Nm]	$M_{max}$ [Nm]	$M_{mean}$ [Nm]	$MAD(M)$ [Nm]	Torque space volume [ $N^3m^3$ ]	Torque space surface [ $N^2m^2$ ]
Optimal	12.85	18.2	16.93	0.7	20'358	3'741
Standard	10.9	21.8	16	1.63	18'409	3'580

### 3.3.3 Hepta-copter

Optimal hepta-copter:

Table 3.12: Comparison between two designs' hover capabilities.

Design	$H_{eff,min}$ [%]	$H_{eff,max}$ [%]	$H_{eff,mean}$ [%]	$MAD(H_{eff})$ [%]
Optimal	80.33	99.4	90.96	3
Standard	77.25	100	84.38	5.2

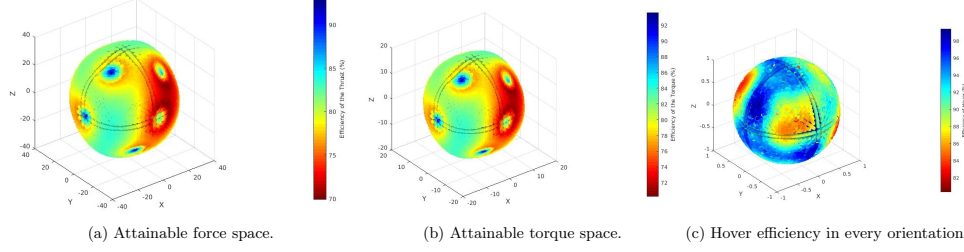


Figure 3.13: Representation of the capacities of the optimal penta-copter.

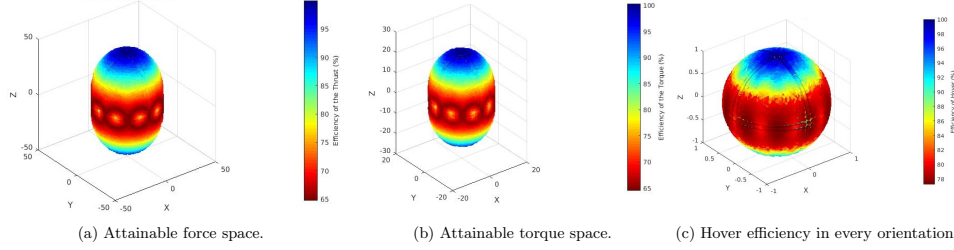


Figure 3.14: Representation of the capacities of the standard penta-copter.

- $n = 7$
- $\beta_{arm} = [35.26^\circ, 35.26^\circ, 35.26^\circ, 35.26^\circ, 35.26^\circ, 35.26^\circ, 35.26^\circ]$
- $\theta_{arm} = [0^\circ, 0^\circ, 0^\circ, 0^\circ, 0^\circ, 0^\circ, 0^\circ]$
- $L = 0.5 \text{ [m]}$

### 3.4 Comparison of Different Designs

Table 3.13: Comparison between all the different optimal designs' force capabilities.

Design	$F_{min}$ [N]	$F_{max}$ [N]	$F_{mean}$ [N]	$MAD(F)$ [N]	Force space volume [ $N^3$ ]	Force space surface [ $N^2$ ]
Tri-copter	17.37	21.27	19.73	1.1	33'217	5'313
Quad-copter	23.23	28.37	26.87	0.86	81'710	9'326
Penta-copter	28.95	35.46	29.39	0.46	107'463	11'130
Hexa-copter	34.74	42.55	39.52	2.21	267'010	20'922
Hepta-copter	39.96	49.44	47.18	0.96	447'344	28'929
Octa-copter	44.7	58.78	53.95	0.94	669'339	37'625

### 3.5 Results when n is an Optimization Parameter

Optimal n-copter sqp algorithm:

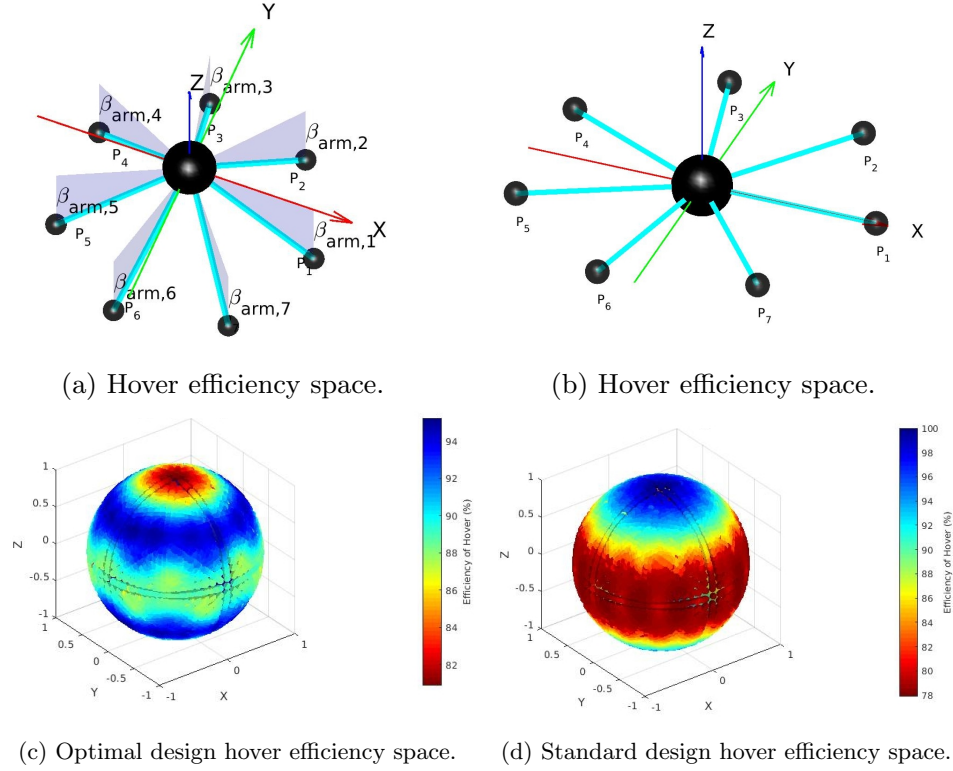


Figure 3.15: Visual representation of the optimal Hepta-copter capabilities.

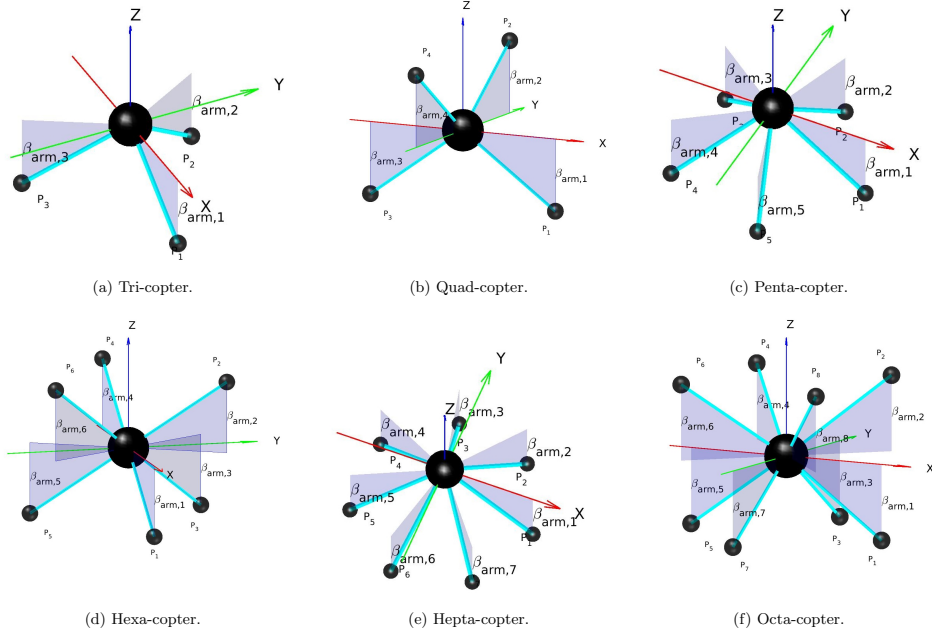


Figure 3.16: Representation of all the optimal designs.

- $n = 3$

Table 3.14: Comparison between all the different optimal designs' torque capabilities.

Design	$M_{min}$ [Nm]	$M_{max}$ [Nm]	$M_{mean}$ [Nm]	$MAD(M)$ [Nm]	Torque space volume [ $N^3 m^3$ ]	Torque space surface [ $N^2 m^2$ ]
Tri-copter	8.7	10.67	9.87	0.56	4'158	1'379
Quad-copter	11.65	14.23	13.47	0.43	10'300	2'348
Penta-copter	14.52	17.78	14.74	0.23	13'555	2'800
Hexa-copter	17.42	21.34	19.82	1.1	33'687	5'230
Hepta-copter	20.04	24.8	23.66	0.48	56'403	7'304
Octa-copter	22.4	29.48	27	0.47	84'417	9'463

Table 3.15: Comparison between all the different optimal designs' hover capabilities.

Design	$H_{eff,min}$ [%]	$H_{eff,max}$ [%]	$H_{eff,mean}$ [%]	$MAD(H_{eff})$ [%]
Tri-copter	81.65	99	87.22	4.42
Quads-copter	81.65	94.73	87.1	2.6
Penta-copter	81.65	91.43	85.35	1.49
Hexa-copter	81.65	100	88.92	4.43
Hepta-copter	80.88	95.23	91.1	2.4
Octa-copter	81.78	96.65	91.42	2.7

- $\beta_{arm} = [36^\circ, 36^\circ, 36^\circ]$
- $\theta_{arm} = [0^\circ, 0^\circ, 0^\circ]$
- $L = 0.4 [m]$

Optimal n-copter genetic algorithm:

- $n = 7$
- $\beta_{arm} = [10.13^\circ, -3.73^\circ, -49.51^\circ, 49.76^\circ, -56.67^\circ, 47.03^\circ, -17.86^\circ]$
- $\theta_{arm} = [-18.93^\circ, -9.51^\circ, 1.22^\circ, 12.93^\circ, 13.58^\circ, 13.07^\circ, -26.33^\circ]$
- $L = 0.5 [m]$

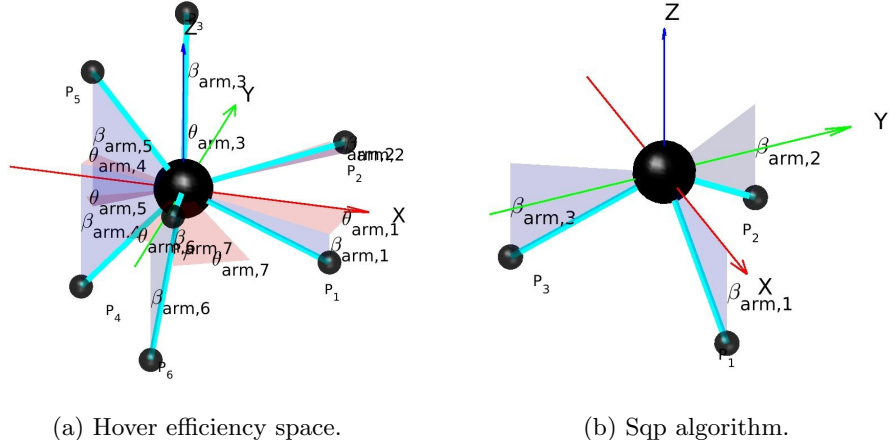


Figure 3.17: Visual representation of the optimal n-copter designs.

## **Chapter 4**

# **Simulation Results**

Evaluate results in simulation.

### **4.1 Hexa-copter**

### **4.2 Hepta-copter**

### **4.3 Octa-copter**



# **Chapter 5**

## **Conclusion**

- 5.1 Summary/Achieved**
- 5.2 Improvements**
- 5.3 Further Developement**



# Bibliography

- [1] M. Silvagni, A. Tonoli, E. Zenerino, and M. Chiaberge, “Multipurpose UAV for search and rescue operations in mountain avalanche events,” *Geomatics, Natural Hazards and Risk*, vol. 8, no. 1, pp. 18–33, Jan. 2017.
- [2] DJI Mavic Pro & Mavic Pro Platinum – Every Creative Moment – DJI. <https://www.dji.com/mavic>. Accessed: 2018-09-03.
- [3] Aura. <https://aura-drone.com/us/>. Accessed: 2010-09-30.
- [4] D. Brescianini and R. D’Andrea, “Design, modeling and control of an omnidirectional aerial vehicle,” in *2016 IEEE International Conference on Robotics and Automation (ICRA)*, May 2016, pp. 3261–3266.
- [5] M. Kamel, S. Verling, O. Elkhatib, C. Sprecher, P. Wulkop, Z. Taylor, R. Siegwart, and I. Gilitschenski, “Voliro: An Omnidirectional Hexacopter With Tilttable Rotors,” *arXiv:1801.04581 [cs]*, Jan. 2018, arXiv: 1801.04581.
- [6] A. Nikou, G. C. Gavridis, and K. J. Kyriakopoulos, “Mechanical design, modelling and control of a novel aerial manipulator,” in *2015 IEEE International Conference on Robotics and Automation (ICRA)*, May 2015, pp. 4698–4703.
- [7] S. Rajappa, M. Ryll, H. H. Bülthoff, and A. Franchi, “Modeling, control and design optimization for a fully-actuated hexarotor aerial vehicle with tilted propellers,” in *2015 IEEE International Conference on Robotics and Automation (ICRA)*, May 2015, pp. 4006–4013.
- [8] “MATLAB,” <https://en.wikipedia.org/w/index.php?title=MATLAB&oldid=852828655>, Jul. 2018, (Online: accessed August 30, 2018).
- [9] “Gazebo,” <http://wiki.ros.org/ROS/Tutorials>, (Online: accessed September 3, 2018).
- [10] “ROS/Tutorials - ROS Wiki,” <http://wiki.ros.org/ROS/Tutorials>, (Online: accessed August 12, 2018).
- [11] M. Ryll, H. H. Bülthoff, and P. R. Giordano, “Modeling and control of a quadrotor UAV with tilting propellers,” in *2012 IEEE International Conference on Robotics and Automation*, May 2012, pp. 4606–4613.
- [12] “Solide de Platon,” [https://fr.wikipedia.org/w/index.php?title=Solide\\_de\\_Platon&oldid=150277971](https://fr.wikipedia.org/w/index.php?title=Solide_de_Platon&oldid=150277971), Jul. 2018, (Online: accessed September 7, 2018).



# Acknowledgements

I would like to thank Prof. Dr. Roland Siegwart for kindly accepting me in his laboratory and allowing me to be a part of this interesting project.  
I would also like to thank my supervisors Karen Bodie and Zachary Taylor for their valuable advice, their help and their availability.



# **Appendix A**

## **UML: Activity Diagram**

